

Vibron-phonon coupling strength in a finite size lattice of H-bonded peptide units

Vincent Pouthier*

Institut UTINAM, Université de Franche-Comté, CNRS UMR 6213, 25030 Besançon Cedex, France

(Received 5 November 2009; published 17 March 2010)

An attempt is made to measure the vibron-phonon coupling strength in a finite size lattice of H-bonded peptide units. Within a finite temperature density matrix approach, we compare separately the influence of both the vibron-phonon coupling and the dipole-dipole interaction on the coherence between the ground state and a local one-vibron state. Due to the confinement, it is shown that the vibron-phonon coupling yields a series of dephasing-rephasing mechanisms that prevents the coherence to decay. Similarly, the dipole-dipole interaction gives rise to quantum recurrences for specific revival times. Nevertheless, intense recurrences are rather rare events so that the coherence behaves as a random variable whose most probable value vanishes. By comparing the degree of the coherence for each interaction, a critical coupling $\chi^*(L)$ is defined to discriminate between the weak and the strong coupling limits. Its size dependence indicates that the smaller the lattice size is, the weaker the vibron-phonon coupling relative to the dipole-dipole interaction is.

DOI: [10.1103/PhysRevE.81.031913](https://doi.org/10.1103/PhysRevE.81.031913)

PACS number(s): 87.10.-e, 71.35.-y, 71.38.Ht, 63.22.-m

I. INTRODUCTION

As first pointed out by Davydov and Kisluka in the 1970s [1], vibrons may play a key role to transfer the energy released by the hydrolysis of adenosine triphosphate in α helices [2–23]. The main idea is that the released energy is initially stored in the high frequency amide-I mode (C=O vibration) of a peptide unit. Then, it delocalizes along the helix due to dipole-dipole interactions and yields vibrational excitons called vibrons. Since each C=O group is engaged in a H bond, a vibron interacts with acoustical phonons that describe the H-bond network dynamics.

According to the Davydov model, the vibron-phonon dynamics in an α helix reduces to that of a single spine of H-bonded peptide units. In such a lattice, the phonons propagate faster than the vibron so that the Davydov model corresponds to the nonadiabatic limit of the Fröhlich Hamiltonian [24]. The quantum nature of the phonons plays a crucial role [5–7] and the vibron dynamics exhibits two asymptotic regimes. In the strong coupling limit, the vibron-phonon coupling predominates over the dipole-dipole interaction. Therefore, the creation of a vibron is accompanied by a lattice distortion, i.e., a contraction of the H bonds surrounding the excited site. The vibron is dressed by a virtual phonon cloud and it forms a small polaron. The dressed basis is obtained by performing a Lang-Firsov transformation [25–29]. However, this transformation is not exact so that a polaron-phonon coupling remains. It favors relaxation and yields an incoherent diffusive motion of the small polaron [17,18,30–33]. By contrast, the weak coupling limit is reached when the dipole-dipole interaction predominates over the vibron-phonon coupling. It is thus more efficient to use a bare basis for characterizing the vibron dynamics. In that case, a standard perturbation theory is applied to treat the coupling with the phonons. Within the nonadiabatic limit, this coupling does not modify the coherent nature of the vibron. The vibron propagates as if it was insensitive to the

phonons and a wavelike vibrational energy flow takes place along the lattice [19,20].

These features reveal that the vibron-phonon coupling strength, i.e., the so-called χ parameter, plays a central role to define the more efficient way to comprehend the vibron properties. However, its value is still under debate. Indeed, most χ values extracted from an indirect comparison between experiments and theories suggest that the strong coupling limit is reached ($|\chi|=30\text{--}62$ pN [4,12,13]). By contrast, estimations of the coupling strength have been carried out by performing *ab initio* calculations for the formamide dimer [34–36]. Most *ab initio* estimates yield smaller χ values, often negative, indicating that the weak coupling limit is reached.

In that context, a simple and intuitive procedure has been established to discriminate between the weak and the strong coupling limits [37]. The main idea is to compare separately the influence of both the vibron-phonon coupling and the dipole-dipole interaction on a one-vibron state that describes the excitation of a given amide-I mode. To account on finite temperature effects, this procedure has been achieved within the vibron reduced density matrix (RDM) approach. Special attention has been paid to characterize the coherence between the zero vibron ground state and a local excited state that generalizes the concept of survival amplitude at finite temperature. We have shown that the vibron-phonon coupling induces dephasing-limited coherent dynamics whereas decoherence occurs due to dipole-dipole interactions since the local excited state couples with neighboring local states. Consequently, our study simply reveals that the strongest interaction is responsible for the fastest decoherence. It provides a critical coupling strength $\chi^*=25$ pN at biological temperature that discriminates between the weak ($\chi < \chi^*$) and the strong ($\chi > \chi^*$) coupling limits.

In the spirit of most theories applied to the Davydov problem, our measure of the coupling strength has been defined in an infinite lattice with translational invariance. However, most proteins have compact and globular shapes due to frequent reversals of the direction of their polypeptide chains [38]. The analysis of the three-dimensional structures of numerous proteins has revealed that they involve a set of sec-

*vincent.pouthier@univ-fcomte.fr

ondary structures, such as α helix and β sheet, connected to each other by common structural elements called β -turn loop. It has been shown, from the Brookhaven Protein Data Bank, that helices containing from 3 to 15 residues are the most abundant in nature indicating that most proteins involve rather small helices [39]. Consequently, the fundamental question arises whether the finite size of the lattice modifies our measure of the coupling strength. In a confined environment, both the vibron energy spectrum and the phonon energy spectrum exhibit a discrete nature. We thus expect the occurrence of quantum recurrences that will prevent the vibron RDM to decay in the long time limit. Therefore, the purposes of the present paper are to address a comprehensive theory to understand the RDM dynamics in a confined environment and thus to provide a measure of the vibron-coupling strength in a finite size lattice.

This paper is organized as follows. In Sec. II, the vibron-phonon Hamiltonian is defined and the procedure to discriminate between the weak and the strong coupling limits is summarized. Numerical calculations are presented in Sec. III and the results are discussed and interpreted in Sec. IV.

II. THEORETICAL BACKGROUND

A. Model Hamiltonian

Let us consider a one-dimensional (1D) lattice of H-bonded peptide units with N sites. Each site $x=1, \dots, N$ contains an amide-I mode with frequency ω_0 . Restricting our attention to the one-vibron dynamics, the x th amide-I mode is equivalent to a two-level system whose first excited state is denoted $|x\rangle$. The zero-vibron state, defined as the vacuum $|\otimes\rangle$, describes all the amide-I modes in their ground state. The vibron Hamiltonian $H_v=H_A+V_A$ is thus written as

$$H_A = \sum_{x=1}^N \hbar \omega_0 |x\rangle\langle x|, \quad (1)$$

$$V_A = \sum_{x=1}^{N-1} \hbar \Phi [|x+1\rangle\langle x| + |x\rangle\langle x+1|],$$

where H_A describes N independent amide-I modes whereas V_A defines dipole-dipole interactions between neighboring amide-I modes. Note that Φ is the vibron hopping constant. In a finite size lattice, one-vibron states do no longer correspond to Bloch waves with well-defined wave vectors. Indeed, the lattice sides lead to reflections so that the true eigenstates are superimpositions of incident and reflected plane waves. They define N stationary states with quantized wave vectors $K_k=k\pi/L$ and eigenfrequencies $\omega_k=\omega_0+2\Phi \cos(K_k)$, where $k=1, \dots, N$ and $L=N+1$. The vibron dynamics is accounted by the free propagator $G(t)=\exp(-iH_v t/\hbar)$ defined as

$$G_{xx'}(t) = \frac{2}{L} \sum_{k=1}^N \sin(K_k x) \sin(K_k x') e^{-i\omega_k t}. \quad (2)$$

A vibron interacts with the phonons that describe the motions of the peptide units connected through hydrogen bonds.

To mimic the fact that a real α helix in a globular protein is embedded in its protein matrix, we assume that the peptide units are confined between two potential wells. As a result, the phonon Hamiltonian is written as

$$H_B = \sum_{x=1}^N \frac{p_x^2}{2M} + \sum_{x=1}^{N-1} \frac{W}{2} (u_{x+1} - u_x)^2 + \frac{W}{2} (u_1^2 + u_N^2), \quad (3)$$

where M is the mass of each peptide unit whose displacement and momentum are u_x and p_x , respectively, and where W is the H bond force constant. The last two terms in Eq. (3) account for the coupling between the side groups $x=1$ and $x=N$ and the protein matrix supposed to be rigid. To simplify our discussion, these couplings are characterized by the force constant W so that the lattice is equivalent to a 1D chain with fixed boundary conditions. Due to the confinement, a stationary regime takes place and the phonon eigenstates correspond to N normal modes with quantized wave vectors $q_p=p\pi/L$, where $p=1, \dots, N$. The corresponding frequencies are $\Omega_p=\Omega_c \sin(p\pi/2L)$, where $\Omega_c=\sqrt{4W/M}$. Within this normal mode representation, the phonon Hamiltonian [Eq. (3)] is rewritten in terms of the standard phonon operators a_p^\dagger and a_p as $H_B=\sum_{p=1}^N \hbar \Omega_p (a_p^\dagger a_p + 1/2)$.

According to the Davydov model, the phonon bath yields random fluctuations of the internal frequency of each amide-I mode. The vibron-phonon coupling Hamiltonian is thus written as

$$V_B = \sum_{x=1}^N \sum_{p=1}^N \hbar \Delta_{px} (a_p^\dagger + a_p) |x\rangle\langle x|, \quad (4)$$

where Δ_{px} is defined as

$$\Delta_{px} = 2\Delta_0 \sqrt{\frac{2}{L} \sin\left(\frac{p\pi}{2L}\right) \cos\left(\frac{p\pi}{2L}\right) \cos\left(\frac{p\pi x}{L}\right)}. \quad (5)$$

In Eq. (5), $\Delta_0=\chi(\hbar^2 MW)^{-1/4}$ depends linearly on the coupling parameter χ introduced in the original Davydov model. Note that the small polaron binding energy $E_B=2\Delta_0^2/\Omega_c=\chi^2/\hbar W$ provides also a measure of the coupling strength.

The vibron-phonon dynamics is governed by the full Hamiltonian $H=H_A+H_B+V_A+V_B$ whose Hilbert space can be partitioned into independent subspaces $E=E_0\oplus E_1$, where E_v denotes the v -vibron subspace. Equations (1) and (4) show that V_A and V_B act in E_1 , only.

B. Measuring the vibron-phonon coupling strength

In this section, a summary of the formalism detailed in Ref. [37] is presented by including the modifications required to describe the dynamics in a confined lattice. To discriminate between the weak and the strong coupling limits, the main idea is to compare separately the influence of V_A and V_B on a one-vibron eigenstate of the unperturbed Hamiltonian $H_0=H_A+H_B$. To proceed, a density matrix formalism [40] is applied to account on finite temperature effects that play a key role in proteins under physiological conditions. The phonons are thus assumed to form a thermal bath whose quantum state is described by the standard Boltzmann distri-

bution ρ_B . In contrast, the amide-I vibrations are prepared in the state $|\Psi_v\rangle = c_0|\otimes\rangle + c_1|x_0\rangle$ ($|c_0|^2 + |c_1|^2 = 1$) which defines a superimposition between the ground state and a local excited state. The initial state of the vibron-phonon system is thus specified by the full density matrix $\rho = |\Psi_v\rangle\langle\Psi_v| \otimes \rho_B$. Therefore, the vibron RDM element that measures the coherence between $|\otimes\rangle$ and $|x_0\rangle$ is equivalent to the survival amplitude of the initial state of the lattice at finite temperature. When V_α is turned on, with $\alpha=A$ or B , this coherence is defined as

$$\sigma_\alpha(x_0 \otimes, t) = \langle x_0 | \text{Tr}_B [e^{-(i/\hbar)(H_0+V_\alpha)t} \rho e^{(i/\hbar)(H_0+V_\alpha)t}] | \otimes \rangle, \quad (6)$$

where Tr_B is a trace over the phonon degrees of freedom.

When $V_\alpha = V_A$, the vibron does not interact with the phonon bath. Its dynamics is governed by the Hamiltonian H_v so that $\sigma_A(x_0 \otimes, t)$ is expressed in terms of the vibron propagator [Eq. (2)] as

$$\sigma_A(x_0 \otimes, t) = G_{x_0 x_0}(t) c_1 c_0^*. \quad (7)$$

When $V_\alpha = V_B$, the time-convolutionless master equation approach is applied [17–20,41–47] so that $\sigma_B(x_0 \otimes, t)$ is expressed as

$$\sigma_B(x_0 \otimes, t) = e^{-i\omega_0 t} \exp \left[- \int_0^t d\tau \Gamma_{x_0}(\tau) \right] c_1 c_0^*. \quad (8)$$

The relaxation operator $\Gamma_{x_0}(t)$ is written as

$$\Gamma_{x_0}(t) = \int_0^t d\tau C_{x_0}(\tau), \quad (9)$$

where $C_x(\tau)$ is the vibron-phonon coupling correlation function defined as [see Eq. (4)]

$$C_x(t) = \sum_p \Delta_{px}^2 [(2n_p + 1) \cos(\Omega_p t) - i \sin(\Omega_p t)], \quad (10)$$

with $n_p = [\exp(\hbar\Omega_p/k_B T) - 1]^{-1}$, k_B being the Boltzmann constant.

In an infinite lattice, $\sigma_A(x_0 \otimes, t)$ [Eq. (7)] decreases over a time scale of about the vibron correlation time $\tau_v = 1/2\Phi$. This correlation time measures the delay needed to the vibron to cover a lattice site and thus to leave the excited state. It defines the time during which the initial coherence survives. In contrast, Eq. (8) describes dephasing-limited coherent dynamics due to the vibron-phonon coupling. This coupling induces random fluctuations of the local excited state energy which destroy the coherence $\sigma_B(x_0 \otimes, t)$. In that context, our measure of the coupling strength has been defined as follows [37]. Let ϵ be the parameter defined in terms of the dephasing rate $\gamma(t) = \text{Re} \Gamma_{x_0}(t)$ as

$$\epsilon = \int_0^{\tau_v} dt \gamma(t). \quad (11)$$

When $\epsilon \ll 1$, $\sigma_A(x_0 \otimes, t)$ decays faster than $\sigma_B(x_0 \otimes, t)$. The dipole-dipole interaction predominates over the vibron-phonon coupling and the weak coupling limit is reached. By contrast, when $\epsilon \gg 1$, $\sigma_B(x_0 \otimes, t)$ decays faster than $\sigma_A(x_0 \otimes, t)$. The opposite situation takes place and the strong coupling limit is reached.

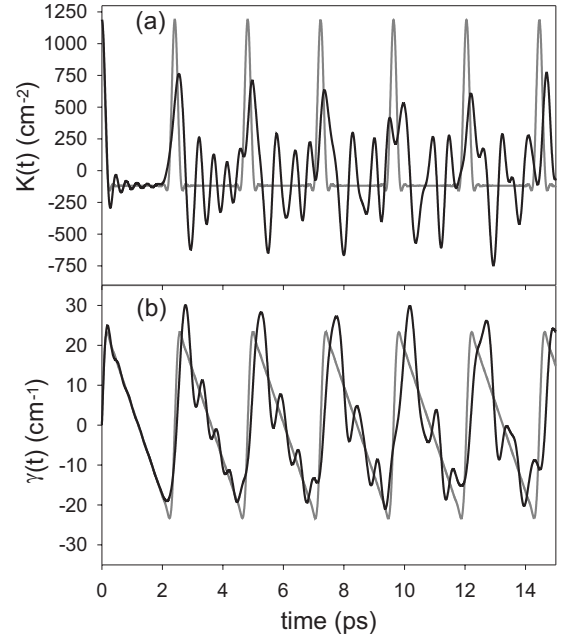


FIG. 1. Time evolution of (a) $K(t)$ and (b) $\gamma(t)$ for $\chi=30$ pN, $T=310$ K, and $L=22$. Gray lines correspond to the Debye model (see the text).

As it will be shown in the following sections, a fully different behavior takes place in a confined environment. Mainly due to the ability of both the vibron and the phonons to be reflected by the lattice sides, $\sigma_A(x_0 \otimes, t)$ and $\sigma_B(x_0 \otimes, t)$ do no longer tend to zero in the long time limit. Time recurrences occur so that the coherent nature of the initial state is more or less restored. Nevertheless, as unbelievable as it seems, we are going to show that our measure of the coupling strength still remains valid when the lattice size is not too small.

III. NUMERICAL RESULTS

In this section, the previous formalism is applied to characterize the vibron-phonon coupling strength in a finite size lattice of H-bonded peptide units. To proceed, typical values for the parameters are used: $\omega_0 = 1660$ cm^{-1} , $\Phi = 7.8$ cm^{-1} , $W = 15$ N m^{-1} , and $M = 1.8 \times 10^{-25}$ kg. The phonon cutoff frequency is $\Omega_c = 96.86$ cm^{-1} so that the adiabaticity $B = 2\Phi/\Omega_c$ is about 0.16. The vibron correlation time is $\tau_v = 0.34$ ps. The temperature is fixed to 310 K unless otherwise stated. Finally, to simplify the discussion, the lattice size L is assumed to be an even number and $x_0 = L/2$.

The time evolution of the coupling correlation function $K(t) = \text{Re} C_{x_0}(t)$ is illustrated in Fig. 1(a) ($\chi=30$ pN and $L=22$). In the short time limit, $K(t)$ behaves as in an infinite lattice. It shows a peak centered on $t=0$ whose amplitude is 1188.70 cm^{-2} . Then, $K(t)$ decays over a time scale of about 0.11 ps by exhibiting small amplitude damped oscillations. Nevertheless, it does not vanish and it converges to a negative value of about -118.0 cm^{-2} . A second peak appears at $t=2.55$ ps. Its amplitude is equal to 761.59 cm^{-2} and its width is about 0.34 ps. After this peak, $K(t)$ decreases again

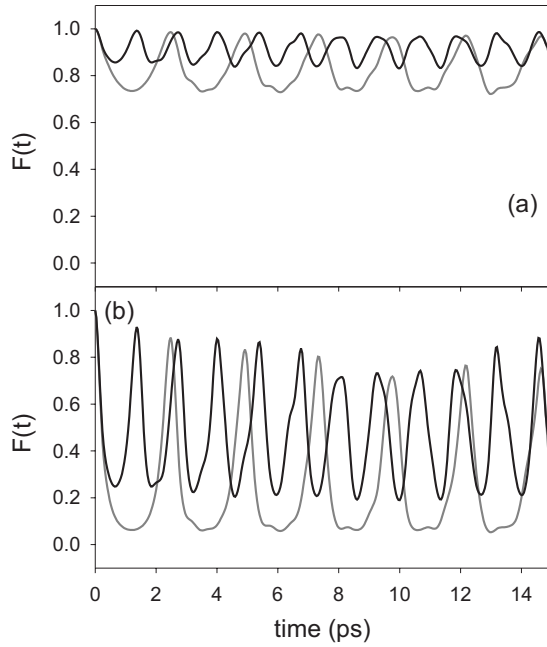


FIG. 2. Time evolution of the decoherence factor for $T=310$ K and for (a) $\chi=10$ pN and (b) $\chi=30$ pN. Black lines correspond to $L=12$, whereas gray lines refer to $L=22$.

by exhibiting damped oscillations around the same negative value. As time passes, similar features are observed and $K(t)$ shows a series of peaks more or less regularly distributed.

As shown in Fig. 1(b), the dephasing rate $\gamma(t)$ exhibits a jerk-and-jump time evolution. Initially equal to zero, $\gamma(t)$ first increases linearly with time to reach a maximum value equal to 24.97 cm^{-1} at $t=0.19$ ps. Then, it decreases almost linearly and reaches a minimum value of about -19.04 cm^{-1} at $t=2.14$ ps. Note that $\gamma(t)=0$ at $t=1.21$ ps. As time increases, $\gamma(t)$ increases again and it vanishes again at $t=2.47$ ps. This scenario continues so that the dephasing rate behaves almost periodically [48] and it shows a series of positive and negative values.

The time evolution of $\sigma_B(x_0 \otimes t)$ is characterized by the decoherence factor $F(t)=\exp[-\int_0^t d\tau \gamma(\tau)]$ whose behavior is illustrated in Fig. 2. For $\chi=10$ pN [Fig. 2(a)], $F(t)$ is an almost periodic function. Its main period increases linearly with the lattice size from 1.34 ps for $L=12$ (black line) to 2.46 ps for $L=22$ (gray line). Initially equal to unity, $F(t)$ decreases according to a Gaussian law in the very short time limit. Then, a slowdown in its decay occurs and $F(t)$ reaches a minimum value F_m that decreases with L . For $L=12$, the first minimum $F_m=0.85$ occurs at $t=0.67$ ps. In contrast, for $L=22$, the minimum $F_m=0.73$ takes place at $t=1.23$ ps. As time passes, $F(t)$ increases and it reaches a maximum whose value is rather close to unity. Such a behavior continues almost periodically so that $F(t)$ varies between a maximum value and a minimum value that remains about $F_m \forall t$. Similar features take place for $\chi=30$ pN [Fig. 2(b)]. Indeed, $F(t)$ still oscillates between a minimum and a maximum value. The minimum values are almost time independent and they are typically of about $F_m=0.25$ for $L=12$ and $F_m=0.06$ for $L=22$. In contrast, the maximum value slightly varies with time although it remains close to unity. The main

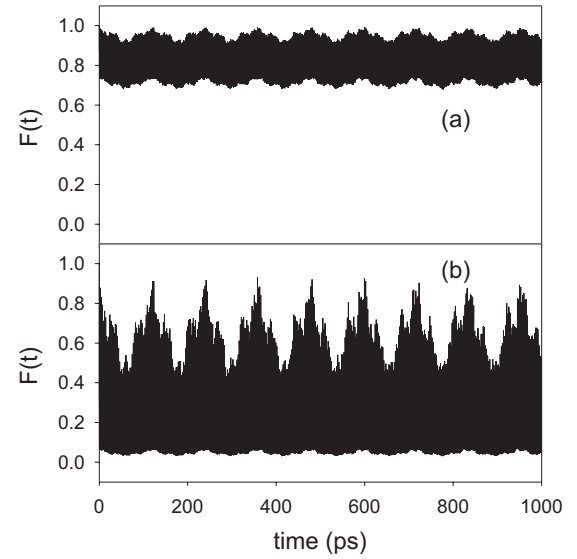


FIG. 3. Time evolution of the decoherence factor for $T=310$ K and $L=22$. (a) $\chi=10$ pN and (b) $\chi=30$ pN.

period of $F(t)$ is χ independent and it reduces to the period observed in Fig. 2(a).

The evolution of $F(t)$ over a larger time scale is illustrated in Fig. 3 for $L=22$. For $\chi=10$ pN [Fig. 3(a)], $F(t)$ exhibits low-frequency oscillations that support a high-frequency small amplitude modulation. The high-frequency component refers to the short time behavior of $F(t)$ described in Fig. 2(a). The low-frequency component exhibits a rather small amplitude that appears almost size independent. Its main period only depends on the lattice size. However, this period does no longer scale linearly with L and it typically varies from 20 ps for $L=12$ (not drawn) to 120 ps for $L=22$. A slightly different behavior occurs for $\chi=30$ pN [Fig. 3(b)]. Indeed, $F(t)$ still involves the mixing between a low-frequency component and a high-frequency component, this latter component referring to the short time behavior observed in Fig. 2(b). However, the low-frequency component yields an asymmetric modulation of the decoherence factor. Although its minimum value is not significantly modified and remains close to $F_m \forall t$, the low-frequency modulation strongly affects its maximum value. This effect is enhanced as L increases so that the maximum value of $F(t)$ typically ranges between 0.7 and 1 for $L=12$ (not drawn) whereas it extends from 0.4 to unity for $L=22$. Note that the main period of these low-frequency oscillations is χ independent. It reduces to the period observed in Fig. 3(a).

The almost periodic behavior observed in Fig. 3 yields an apparent randomness of $F(t)$ whose properties can be investigated by performing a statistical analysis. To proceed, $F(t)$ can be viewed as a realization of a random variable F . Over a sufficiently long time scale \mathcal{T} , the curve $F(t)$ defines a sample over which statistical quantities can be computed in an empirical way, i.e., without deploying a statistical model. Note that \mathcal{T} is assumed to be sufficiently long so that the ergodic principle can be applied, i.e., all the possible realizations of the random variable F are assumed to occur over the range $[0, \mathcal{T}]$. Within this point of view, the distribution $g(F)$ is displayed in Fig. 4. For $\chi=10$ pN [Fig. 4(a)], $g(F)$ is

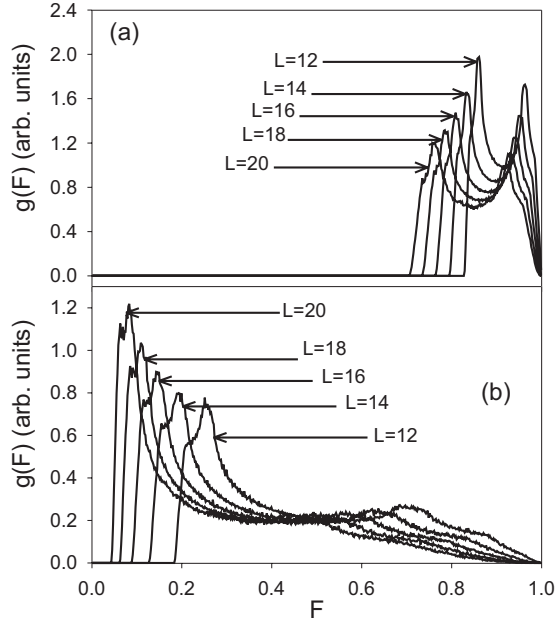


FIG. 4. Distribution of the decoherence factor for $T=310$ K. (a) $\chi=10$ pN and (b) $\chi=30$ pN. The simulation has been carried out over 5000 ps with 5×10^5 time steps.

almost uniform over the range $[F_M, 1]$, where F_M decreases from 0.83 for $L=12$ to 0.70 for $L=20$. More precisely, $g(F)$ exhibits two peaks. The first peak is close to unity. It is slightly shifted when L increases and its position varies from 0.96 for $L=12$ to 0.92 for $L=22$. The second peak is more sensitive to the lattice size. It decreases from 0.86 for $L=12$ to 0.76 for $L=20$. In fact, the position of this latter peak corresponds to the minimum decoherence factor F_m observed in the short time limit [Fig. 2(a)]. When $\chi=30$ pN [Fig. 4(b)], $g(F)$ becomes broader. The peak close to unity tends to disappear whereas the second peak, which remains centered around F_m [see Fig. 2(b)], becomes more intense. This peak moves closer to zero when both L and χ increase.

With the ingredients that define $\sigma_B(x_0 \otimes t)$ being characterized, let us now focus our attention on the coherence $\sigma_A(x_0 \otimes t)$ that describes the survival amplitude of the local excited state $|x_0\rangle$ when the dipole-dipole interaction is turned on [Eq. (7)]. Information about this local coherence is extracted from the survival probability $P(t) = |G_{x_0 x_0}(t)|^2$ whose behavior is displayed in Fig. 5 for $L=16$.

When $t < 4$ ps, $P(t)$ behaves as in an infinite lattice so that its evolution is governed by the vibron correlation time ($\tau_v = 0.34$ ps). Initially equal to unity, $P(t)$ decreases with time. It reaches a value of about 0.60 when $t = \tau_v$, indicating that 40% of the population of the excited site have been transferred to neighboring sites. Nevertheless, $P(t)$ does not vanish in the long time limit. Due to the confinement, the memory of the initial vibron state is more or less recovered as time increases. Indeed, over a rather short time scale [Fig. 5(a)], $P(t)$ exhibits peaks which are almost periodically distributed. These peaks take place at $t=5.77$ ps, $t=10.80$ ps, and $t=16.60$ ps and the corresponding amplitudes are equal to 0.40, 0.43, and 0.60. They characterize quantum recurrences that occur at specific revival times. Nevertheless,

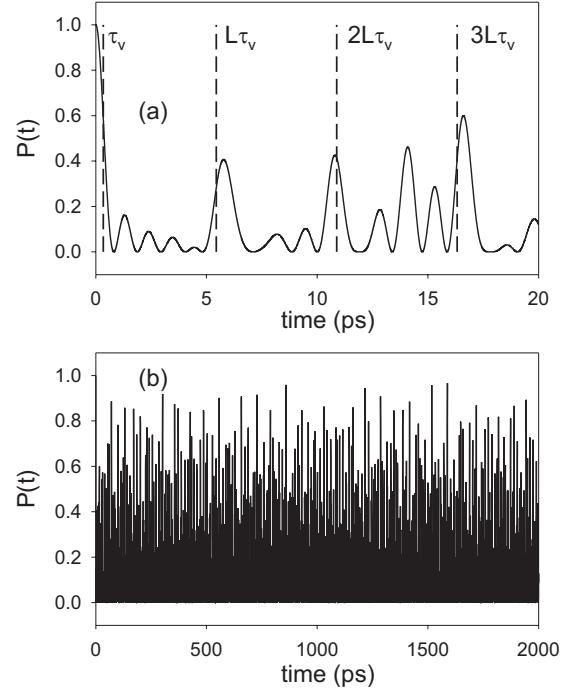


FIG. 5. Time evolution of the survival probability $P(t) = |G_{x_0 x_0}(t)|^2$ for $L=16$.

these recurrences define quantum states that only slightly resemble the initial local state. Less than or about to 60% of the initial population recurs on the excited site, the remaining population being delocalized over the other sites. Over a time scale equal to 200 ps (not drawn), $P(t)$ exhibits a series of peaks, most of which are characterized by an amplitude smaller than 0.60. Between two successive peaks, $P(t)$ shows high-frequency small amplitude oscillations. Nevertheless, eight peaks whose amplitude is larger than 0.60 have been observed. As shown in Fig. 5(b), similar features occur over 2000 ps. The curve $P(t)$ shows a series of discrete peaks more or less intense that emerges from a continuous background. The number of intense quantum recurrences increases and 29 peaks whose amplitude is larger than 0.8 are clearly observed. For instance, $P(t)=0.88$ at $t=70.82$ ps and it reaches 0.97 at $t=1588.20$ ps. These intense peaks occur at revival times for which the initial coherence almost recurs exactly. They thus describe quantum recurrences for which the vibron quantum state strongly resembles the initial state with only a phase factor.

The occurrence of quantum recurrences that emerge for a continuous background provides a random nature to $P(t)$. Consequently, in analogy with our study of the decoherence factor, the behavior of the survival probability can be investigated by performing a statistical analysis. In that context, the distribution $g(P)$ is displayed in Fig. 6. This distribution is independent of the vibron hopping constant. It only depends on the lattice size, and, for rather large L values [Fig. 6(b)], $g(P)$ scales as a power law $g(P) \approx P^{-\alpha}$ whose exponent is about $\alpha \approx 0.7$. This feature indicates that $P=0$ is the most probable value of the survival probability. The mean value of P decreases with the lattice size and it reduces to $2/L$. Similarly, the second moment also scales as $2/L$ in

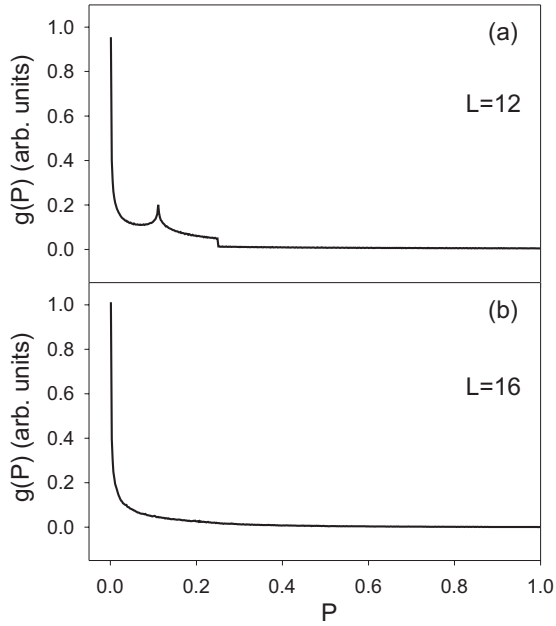


FIG. 6. Distribution of the survival probability for (a) $L=12$ and (b) $L=16$. The simulation has been carried out over 5000 ps with 5×10^5 time steps.

accordance with the fact that $g(P)$ is strongly peaked on $P=0$. Nevertheless, for smaller L values, a slightly different behavior takes place. When $L=12$ [Fig. 6(a)], in addition to the main peak that occurs for $P=0$, $g(P)$ exhibits a second peak for $P=0.11$. This latter peak is about five times smaller than the main peak, so that $P=0$ still remains the most probable value. The presence of this additional peak is responsible for a broadening of the distribution. This second peak disappears when $L=10$ and $L=8$ but it recurs when $L=6$. In that case, $g(P)$ supports a third peak centered on unity. The second and the third peaks are about two times and three times smaller than the main peak still centered on $P=0$. Finally, when $L=4$ a fully different behavior occurs since $g(P)$ shows two peaks with the same amplitude and centered on zero and on unity. This case corresponds to a special situation in which $P(t)$ is a true periodic function.

These results show that $\sigma_A(x_0 \otimes t)$ exhibits intense recurrences that correspond to rather rare events which occur randomly provided that $L > 4$. Therefore, the most probable value of $\sigma_A(x_0 \otimes t)$ vanishes as in an infinite lattice. In other words, the vibron correlation time τ_v remains the relevant time scale over which $\sigma_A(x_0 \otimes t)$ survives in a statistical sense. Consequently, the procedure established in an infinite lattice still remains valid to measure the vibron-phonon coupling strength. In that context, from the knowledge of the decoherence factor we can compute the parameter $\epsilon = -\ln[F(\tau_v)]$ and then extract the critical value of the coupling strength $\chi^*(L)$ that discriminates between the weak coupling limit [$\chi < \chi^*(L)$] and the strong coupling limit [$\chi > \chi^*(L)$]. For $L \geq 6$, the dependence of the critical coupling $\chi^*(L)$ with respect to the lattice size is illustrated in Fig. 7. The figure reveals that $\chi^*(L)$ exhibits two regimes whatever the temperature. For large L values, $\chi^*(L)$ is a slowly decaying function of the lattice size that converges to a constant value when L tends to infinity. We thus recover the

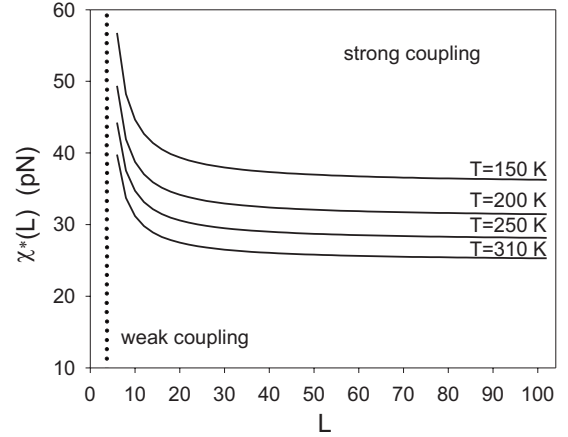


FIG. 7. Size dependence of the critical coupling $\chi^*(L)$.

behavior of the critical coupling in an infinite lattice and $\chi^*(L \rightarrow \infty)$ increases when the temperature decreases. For $L=102$, it ranges between 25.29 and 36.25 pN when T reduces from 310 to 150 K. However, when L decreases, $\chi^*(L)$ increases whatever the temperature. At $T=310$ K, they are equal to 27.83, 28.90, 31.20, and 39.77 pN when L is successively equal to 18, 14, 10, and 6. Note that a divergence seems to occur when L reaches a critical value of about $L \approx 4$. Nevertheless, in that case, our measure of the coupling strength breaks down since the survival probability $P(t)$ is a true periodic function (see the discussion of Fig. 6).

IV. DISCUSSION

In a finite size lattice, the numerical results reveal that the coherence $\sigma_B(x_0 \otimes t)$ evolves almost periodically when the vibron-phonon coupling is turned on. The decoherence factor does not vanish in the long time limit but it oscillates, according to at least two time scales, between a minimum F_m and a maximum close to unity. From a statistical point of view, F_m is typically the most probable value of the decoherence factor. It decreases with both L and χ indicating that the larger the lattice size and the vibron-phonon coupling are, the smaller the degree of the coherence is. Similarly, the finite size of the lattice induces quantum recurrences in the time evolution of the coherence $\sigma_A(x_0 \otimes t)$. Nevertheless, provided that $L > 4$, intense recurrences correspond to rather rare events that appear more or less randomly. They are not representative of the behavior of the coherence whose most probable value is zero, as in an infinite lattice. This means that $\sigma_A(x_0 \otimes t)$ survives, in a statistical sense, over a time scale of about the vibron correlation time. The main consequence is that the procedure established in an infinite lattice still remains valid when the lattice size is not too small. However, this procedure has now a statistical meaning and it allows us to compare the degree of the vibronic coherence when either V_A or V_B is turned on. In other words, when $\epsilon \ll 1$, the coherence $\sigma_B(x_0 \otimes t)$ remains close to its initial value whereas $\sigma_A(x_0 \otimes t)$ vanishes in a statistical sense. The dipole-dipole interaction predominates over the vibron-phonon coupling and the weak coupling limit is reached. In contrast, when $\epsilon \gg 1$, the opposite situation occurs indicating

that the strong coupling limit is reached. From the equation $\epsilon=1$, a critical coupling $\chi^*(L)$ has been identified to characterize the transition between the weak and the strong coupling limits. The main point is that $\chi^*(L)$ increases when L decreases indicating that the vibron-phonon coupling decreases relative to dipole-dipole interactions when the confinement is enhanced.

To interpret these observed features, let us first investigate the way the vibron-phonon coupling affects the vibronic coherence. To proceed, the so-called Debye model is applied so that the phonon dispersion curve is linearized according to the relation $\Omega_p \approx \Omega_c p \pi / 2L$ [18,19]. Within this model, the coupling correlation function $K(t)$ at biological temperature is expressed as

$$K(t) = 2E_B \bar{k}_B T [\phi_L(t) + \phi_L(t + T_0)], \quad (12)$$

where $\bar{k}_B = k_B / \hbar$, $T_0 = L \tau_c$, and $\tau_c = 2 / \Omega_c$ is the phonon correlation time. In Eq. (12), $\phi_L(t) = f_L(t) + 1/2 f_L(t + \tau_c) + 1/2 f_L(t - \tau_c)$ involves the function $f_L(t)$ defined as

$$f_L(t) = \frac{1}{L} \cos\left(\frac{\pi N t}{2L \tau_c}\right) \frac{\sin\left(\frac{\pi t}{2\tau_c}\right)}{\sin\left(\frac{\pi t}{2L \tau_c}\right)} - \frac{1}{L}. \quad (13)$$

Equation (12) reveals that $K(t)$ is a T_0 -periodic function which exhibits a series of peaks whose amplitude is $2E_B \bar{k}_B T(1 - 2/L)$ and whose width is about $2\tau_c$ [see gray line in Fig. 1(a)]. With the parameters used in the simulation, the peak amplitude is equal to 1183.24 cm^{-2} whereas the period is $T_0 = 2.41 \text{ ps}$ ($\tau_c \approx 0.11 \text{ ps}$ and $L = 22$). Between two successive peaks, $K(t)$ does not vanish. It is equal to a negative value $-4E_B \bar{k}_B T / L$ which is about -118.32 cm^{-2} . In other words, over a single period ($0 < t < T_0$), $K(t)$ scales as (with $\bar{t} = t / \tau_c$)

$$K(t) \approx \begin{cases} 2E_B \bar{k}_B T(1 - 2/L) & \text{if } \bar{t} \leq 1 \\ -4E_B \bar{k}_B T / L & \text{if } 1 \leq \bar{t} \leq N \\ 2E_B \bar{k}_B T(1 - 2/L) & \text{if } N \leq \bar{t} \leq L. \end{cases} \quad (14)$$

Since $\dot{\gamma}(t) = K(t)$ [Eq. (9)], the integration of Eq. (14) provides an analytical expression of the dephasing rate. This procedure reveals that $\gamma(t)$ is also a T_0 -periodic function defined as

$$\gamma(t) \approx \gamma_0 \begin{cases} \left(1 - \frac{2}{L}\right) \frac{t}{\tau_c} & \text{if } \bar{t} \leq 1 \\ -\left(\frac{2t}{T_0} - 1\right) & \text{if } 1 \leq \bar{t} \leq N \\ \left(1 - \frac{2}{L}\right) \frac{t - T_0}{\tau_c} & \text{if } N \leq \bar{t} \leq L, \end{cases} \quad (15)$$

where $\gamma_0 = 4E_B \bar{k}_B T / \Omega_c$ is the dephasing rate in an infinite lattice [37]. Equation (15) shows that $\gamma(t)$ varies periodically between two size dependent values $\pm \gamma_L$, with $\gamma_L = \gamma_0(1 - 2/L)$. In the short time limit, $\gamma(t)$ increases from zero to reach $+\gamma_L$ at $t = \tau_c$. Dephasing-limited coherent dy-

namics occurs. However, when $\tau_c < t < T_0 - \tau_c$, $\gamma(t)$ decreases linearly with time. It remains positive provided that $t < T_0/2$ indicating a slowdown in the decoherence process. Then, when $t > T_0/2$, $\gamma(t)$ becomes negative so that a rephasing mechanism takes place. It continues to decay and it reaches $-\gamma_L$ at $t = T_0 - \tau_c$. Finally, as time increases, $\gamma(t)$ remains negative but it increases with time and vanishes at $t = T_0$. As shown in Fig. 1(b) (gray line), the Debye model provides a theoretical expression for the dephasing rate that mimics quite well the numerical results. It yields $\gamma_L = 24.43 \text{ cm}^{-1}$, in a rather good agreement with the numerical observations.

Within the Debye model, the decoherence factor is a T_0 -periodic function expressed as

$$F(t) \approx \begin{cases} \exp\left[-\frac{\gamma_L t^2}{2\tau_c}\right] & \text{if } \bar{t} \leq 1 \\ \exp\left[-\gamma_0\left(t - \frac{\tau_c}{2} - \frac{t^2}{T_0}\right)\right] & \text{if } 1 \leq \bar{t} \leq N \\ \exp\left[-\frac{\gamma_L(t - T_0)^2}{2\tau_c}\right] & \text{if } N \leq \bar{t} \leq L. \end{cases} \quad (16)$$

When $t < \tau_c$, $F(t)$ decays according to the Gaussian law $F(t) \approx \exp[-E_B \bar{k}_B T(1 - 2/L)t^2]$ indicating that dephasing occurs as in the infinite lattice. However, as time increases, a slowdown in the decay of $F(t)$ is observed. Consequently, at $t = T_0/2$, $F(t)$ reaches a minimum value defined as

$$F_m = \exp\left[-\frac{2E_B \bar{k}_B T}{\Omega_c^2}(L - 2)\right]. \quad (17)$$

As observed in Fig. 2, F_m decreases with both L and χ . For $\chi = 10 \text{ pN}$, it decreases from 0.86 to 0.73 when L ranges between 12 and 22. Similarly, for $\chi = 30 \text{ pN}$, F_m varies from 0.25 to 0.06 when L increases from 12 to 22. Then, over the time scale $T_0/2 < t < T_0$, the decoherence factor increases. It finally reaches unity at time T_0 indicating that the initial coherence is restored. Note that the behavior observed in an infinite lattice is recovered from Eqs. (15) and (16) within the limit $L \rightarrow \infty$ [37].

The Debye model captures the main part of the physics that characterizes the dephasing rate and the decoherence factor. To understand this physics in a simple way, let us assume that the phonon bath is initially in a quantum state $|\Psi_B\rangle$ that corresponds to a well-defined number state for each phonon mode. Note that, in practice, a statistical average is performed to account on finite temperature effects (see Sec. III). In contrast, the vibron state is a superimposition that involves the ground state and a local excited state $|x_0\rangle$. The vibron-phonon state at $t=0$ is thus a tensor product between the two previous quantum states. When the vibron-phonon coupling V_B is turned on, this state evolves in an entangled vibron-phonon state as

$$|\Psi(t)\rangle = c_0 | \otimes \rangle \otimes |\Psi_B^0(t)\rangle + c_1 e^{-i\omega_0 t} |x_0\rangle \otimes |\Psi_B^1(t)\rangle, \quad (18)$$

where $|\Psi_B^0(t)\rangle$ and $|\Psi_B^1(t)\rangle$ are the phonon states at time t when the phonon dynamics is governed by H_B and

$H_B + V_B(x_0 x_0)$, respectively. After performing a trace over the phonon degrees of freedom, $\sigma_B(x_0 \otimes, t) \propto \langle \Psi_B | \Psi_B^1(t) \rangle$ defines the survival amplitude of the initial phonon state when the phonons experience the coupling $V_B(x_0 x_0)$.

This coupling brings each phonon mode in a coherent state. Consequently, the phonons reach a quasiclassical state that corresponds to a lattice distortion, i.e., a contraction of the H bonds surrounding the site x_0 . Since each phonon coherent state evolves in time, the lattice distortion propagates according to two acoustic wave packets that are emitted on each side of the excited site. These wave packets propagate with sound velocity $c = \Omega_c/2$ and they cover a lattice parameter after a time scale of about τ_c . In that context, $K(t)$ measures the lattice memory at time t of the initial distortion, i.e., the memory of the initial phonon state.

Consequently, $K(t)$ takes a significant value when the initial distortion is still localized around the excited site. Then, it decreases after a time scale of about τ_c indicating that the two emitted wave packets have left the excited region. Over this short time scale, the phonon state develops a rather fast evolution so that the phonon bath rapidly loses the memory of its initial state. This memory loss drastically affects the coherent nature of the vibronic superimposition. The corresponding coherence decreases according to a decay rate that increases linearly with time to reach a maximum value γ_L at $t = \tau_c$. This rate depends on the lattice size because the intensity of the vibron-phonon coupling is reduced in a confined environment. A measure of the coupling strength is provided by the parameter $\epsilon_B(L) = \sum_p \Delta_{px}^2 / \Omega_p$ which is equal to $E_B(1-2/L) \forall x$ [29].

When $t > \tau_c$, the phonon state continues to evolve and the two emitted wave packets delocalize far from the excited region. Nevertheless, $K(t)$ does not vanish. It converges to a time independent negative value indicating that the phonon bath slightly keeps the memory of its initial state. Therefore, correlations remain between the initial distortion and the two propagating deformations located around $x_0 \pm ct$. These correlations are mediated by the quantum fluctuations of the lattice site motions when the phonons occupy the initial state $|\Psi_B\rangle$. Note that, at biological temperature, these correlations have a thermodynamics origin since they result from the thermal fluctuations of the lattice site motions. These correlations play a fundamental role since they give rise to a slowdown in the decoherence process. Therefore, dephasing-limited coherent dynamics remains but the corresponding dephasing rate $\gamma(t) = \gamma_0 - 2\gamma_0 t / L\tau_c$ decreases with time due to the confinement.

In fact, because they evolve in a confined lattice, it is as if the phonons knew that they were going to recover their initial state and thus to restore the initial coherence of the vibronic superimposition. Indeed, at $t = T_0/2$, the two wave packets are reflected. They propagate back to the excited region and they reappear simultaneously on x_0 at time T_0 . At that time, $K(t)$ exhibits a new peak indicating that the phonons recover their initial state with only a phase factor. In other words, it is as if the phonon state went back in time after experienced the reflection on the lattice sides. Over this time scale, the dephasing rate becomes negative. A rephasing mechanism takes place that exactly compensates the previous dephasing mechanism. The decoherence factor increases

over a time scale of about $T_0/2$ and, at $t = T_0$, the initial vibronic coherence recurs.

Within the Debye model, the previous scenario shows that a series of dephasing-rephasing mechanisms takes place periodically. However, due to the phonon dispersion, this periodicity is more or less broken. Indeed, the real phonon dispersion curve exhibits a nonlinear dependence with respect to the phonon wave vector. This dispersion is responsible for the spreading of the wave packets so that the initial phonon state is no longer exactly recovered after each reflection. However, because the time evolution of the wave packets is governed by a discrete energy spectrum, quantum recurrences take place [49–53]. The dynamics is thus characterized by so-called revival times for which the two wave packets recur simultaneously in the excited region and provide a quantum state that strongly resembles the initial phonon state. The revival times can be extracted from the Taylor series of the phonon dispersion curve expressed as

$$\Omega_p = \Omega_{p=0} + 2\pi \left(\frac{p}{T_{cl}} + \frac{1}{2!} \frac{p^2}{T_r} - \frac{1}{3!} \frac{p^3}{T_{sr}} + \dots \right), \quad (19)$$

where T_{cl} is the classical time, T_r is the revival time, and T_{sr} is the super-revival time. From the phonon dispersion curve one obtains $T_{cl} = 2L\tau_c$, $T_r = \infty$, and $T_{sr} = 8L^3\tau_c / \pi^2$. Nevertheless, since $x_0 = L/2$, only even phonon modes $p = 2, 4, 6, \dots$ are excited. Consequently, the relevant time scales are no longer T_{cl} and T_{sr} but $T_0 = T_{cl}/2$ and $T_R = T_{sr}/2^3$. For the parameters used in the simulation, one finally obtains $T_0 = 1.31$ ps and $T_R = 19.18$ ps for $L = 12$ whereas $T_0 = 2.41$ ps and $T_R = 118.18$ ps for $L = 22$. In a rather good agreement with the features observed in Fig. 3, T_0 is the period of the high-frequency component of the decoherence factor whose local maxima characterize phonon quantum states that more or less resemble the initial phonon state. In contrast, the super-revival time T_R is the period of the low-frequency component of the decoherence factor whose maxima, close to unity, refer to situations in which the phonon state becomes almost identical to the initial phonon state.

Let us now discuss how the vibronic coherence behaves when the dipole-dipole interaction is turned on. As shown in Eq. (7), this coherence $\sigma_A(x_0 \otimes t)$ is proportional to the diagonal element of the free vibron propagator $G_{x_0 x_0}(t)$ [Eq. (2)]. From a physical point of view, $G_{x_0 x_0}(t)$ defines the probability amplitude to observe the vibron in a state $|x_0\rangle$ at time t given that it occupies this state at $t=0$. It thus measures the lattice memory of the initial vibron state. This memory evolves in time since the vibron delocalizes along the lattice due to dipole-dipole interactions. Indeed, the initial excitation of the vibron yields the emission of two wave packets that propagate with group velocity $v = 2\Phi$ on each side of the excited site x_0 . After a time scale of about τ_v , these wave packets have left the excited region so that the memory decreases and almost vanishes. However, at $t \approx L\tau_v/2$, the wave packets reach the lattice sides, are reflected, and propagate back to the central site. Consequently, the memory recurs at time $T_0 = L\tau_v$, i.e., when the two wave packets reappear simultaneously in the excited region. The vibron

reaches a quantum state that resembles the initial state. As observed in Fig. 5(a), such a mechanism takes place periodically, with a period of about $T_0=5.44$ ps ($L=16$), and it gives rise to the occurrence of quantum recurrences.

Nevertheless, the vibron experiences a strong dispersion that induces a fast spreading of the two propagating wave packets. Consequently, the initial vibron state is only partially recovered after each reflection. However, as the phonon dynamics, the properties of the vibron in a confined environment are governed by a discrete energy spectrum. Therefore one may expect to observe revival times for which the reappearance of the two wave packets in the excited region provides quantum states that strongly resemble the initial vibron state. Information about time revivals can be extracted from the Taylor expansion of the vibron dispersion curve. To proceed, let us assume that the initial wave packet is centered around a quantum number k_0 . The vibron dispersion curve is thus approximated as

$$\omega_k = \omega_{k_0} + 2\pi \left(-\frac{k-k_0}{\mathcal{T}_{cl}} + \frac{1}{2!} \frac{(k-k_0)^2}{\mathcal{T}_r} + \dots \right), \quad (20)$$

where $\mathcal{T}_{cl}=L/[\Phi \sin(k_0\pi/L)]$ is the vibron classical time and $\mathcal{T}_r=L^2/[\Phi\pi \cos(k_0\pi/L)]$ is the vibron revival time. When the initial state consists of many eigenstates close to the band center $\omega=\omega_0$, k_0 is about $L/2$. Consequently $\mathcal{T}_r \rightarrow \infty$ so that the dynamics is dominated by the classical time $\mathcal{T}_{cl} \approx L/\Phi$. In contrast, when the initial state involves eigenstates whose energy is close to the band edges $\omega=\omega_0 \pm 2\Phi$, k_0 is about 0 or L . The relevant time scale is now the revival time $\mathcal{T}_r=L^2/[\Phi\pi]$ since $\mathcal{T}_{cl} \rightarrow \infty$.

Unfortunately, the two previous asymptotic situations mix in a complex manner which prevents the occurrence of intense quantum recurrences. Indeed, since $x_0=L/2$, the initial vibron state involves all the eigenstates characterized by an odd quantum number $k=1,3,5,\dots$. Moreover, each eigenstate occurs with the same weight in the initial wave packet. Consequently, the eigenstates close to both the band center and the band edges participate simultaneously in the vibron dynamics. Since only odd quantum numbers are involved, the relevant time scale is neither \mathcal{T}_{cl} nor \mathcal{T}_r but $\mathcal{T}_{cl}/2$ (for $k_0 \approx L/2 \pm 1$) and $\mathcal{T}_r/4$ (for $k_0 \approx 1$ or N). The signature of these two time scales has clearly been observed in Fig. 5. Nevertheless, these two time scales do not yield exact quantum recurrences since the vibron dispersion curve is neither a linear nor a quadratic function of the wave vector. The main consequence is that the memory exhibits a kind of random time evolution in the course of which intense recurrences correspond to rather rare events. Therefore, from a statistical point of view, these intense recurrences are not representative of the behavior of the coherence $\sigma_A(x_0 \otimes t)$. One can thus conclude that the coherence only survives over a time scale of about τ_v , as in an infinite lattice.

In that context, in spite of the confinement, the vibron correlation time τ_v has a physical meaning so that the procedure established in Ref. [37] still remains valid. It involves the calculation of the parameter $\epsilon = -\ln F(\tau_v)$ from the evaluation of the decoherence factor at time τ_v . The weak coupling limit arises when $\epsilon < 1$, whereas the strong coupling

limit takes place when $\epsilon > 1$. Nevertheless, this measure of the coupling strength must be handled extremely carefully and two main conditions must be fulfilled. First, since it is based on a statistical analysis, our measure requires that $\sigma_A(x_0 \otimes t)$ behaves more or less randomly. However, this condition breaks down when the lattice size is too small because $\sigma_A(x_0 \otimes t)$ becomes a periodic function. More precisely, when $L=4$, two vibron eigenstates with quantum number $k=1$ and $k=3$ govern the time evolution of the vibron propagator. The corresponding frequencies being $\omega_0 \pm \sqrt{2}\Phi$, the coherence $\sigma_A(x_0 \otimes t)$ is proportional to $\cos(\sqrt{2}\Phi t)$. Exact recurrences appear so that the coherence survives over an infinite time scale. It is thus difficult to say if whether or not the dipole-dipole interaction predominates over the vibron-phonon coupling. The second condition stipulates that our measure is valid if and only if the adiabaticity B belongs to a given interval. Indeed, the nonadiabatic limit is reached provided that $B \leq B_c$, with $B_c=0.5$, so that $\tau_c < \tau_v$ [20]. Moreover, due to the periodic nature of the decoherence factor, τ_v must be at least shorter than $T_0/2$. As a result, the adiabaticity is bounded from below, i.e., $B \geq B_m$ with $B_m=1/L$. Situations in which $\tau_v > T_0/2$ will provide a paradox. For instance, a small Φ value and a large Φ value can yield two vibron correlation times whose associated ϵ parameters are identical.

Therefore, by assuming $L \geq 6$ and $B \in [B_m, B_c]$, the parameter ϵ can be extracted from the decoherence factor over the time scale $t \in [\tau_c, T_0/2]$ [Eq. (16)]. Then, solving the equation $\epsilon=1$ yields the critical coupling as

$$\chi^*(L) = \chi_0 \left[\frac{BL}{(1-B)(L-L^*)} \right]^{1/2}, \quad (21)$$

where $L^*=1/[2B(1-B)]$ and $\chi_0=\hbar W/\sqrt{Mk_B T}$. We have verified that Eq. (21) provides a very good approximation for the numerical results shown in Fig. 7. It reveals that $\chi^*(L)$ increases with the adiabaticity and it extends from $\chi_0\sqrt{2/(L-2)}$ to $\chi_0\sqrt{L/(L-2)}$ when B varies from B_m to B_c . Note that for a fixed L value, the curve $\chi^*(L)$ vs B lies above the critical curve that characterizes an infinite lattice. In contrast, as in an infinite lattice, $\chi^*(L)$ decreases with the temperature according to the law $\chi^*(L) \propto 1/\sqrt{T}$. These features indicate that the larger the T is and the smaller the Φ is, the stronger the vibron-phonon coupling strength is. Note that although $\chi^*(L)$ seems to behave singularly when $L \approx L^*$, no divergence takes place since $B \geq B_m$.

Finally, Eq. (21) allows us to understand the way the critical coupling depends on the lattice size. On the one hand, when $L \rightarrow \infty$, $\chi^*(L)$ tends to $\chi_0\sqrt{B/(1-B)}$ which corresponds to the critical value in an infinite lattice. Since B_m tends to zero, the procedure established in Ref. [37] is recovered. On the other hand, as observed in Fig. 7, $\chi^*(L)$ increases when L decreases. Consequently, for a fixed set of the relevant parameters of the model, the vibron-phonon coupling strength decreases relative to dipole-dipole interactions when the size of the lattice is reduced. This feature originates from the behavior of the decoherence factor that oscillates between unity and a minimum value F_m [Eq. (17)]. This time evolution indicates that a series of dephasing-rephasing mecha-

nisms governs the vibron dynamics. When L decreases, F_m increases because each dephasing-rephasing process occurs over a shorter time scale. Therefore, the dephasing is too weak to strongly modify the degree of the coherence that remains close to its initial value. In other words, the smaller the lattice size is, the weaker the decoherence induced by the phonon bath is.

V. CONCLUSION

In this paper, an attempt has been made to measure the vibron-phonon coupling, relative to the dipole-dipole interaction, in a finite size lattice of H-bonded peptide units. In such a lattice, the vibron dynamics originates in the interplay between the coupling with the phonons, which induces its localization according to a polaron mechanism, and the dipole-dipole interaction, which favors its delocalization. In both cases, each interaction tends to modify the nature of a local one-vibron state corresponding to the excitation of a given amide-I mode. Therefore, to measure the coupling strength, we have compared separately the influence of each interaction on a local excited state. To account on finite temperature effects, this procedure has been achieved by studying a specific element of the vibron RDM that characterizes the coherence between the zero-vibron ground state and a local one-vibron state.

We have shown that under the vibron-phonon coupling the vibronic coherence measures the survival amplitude of the initial phonon state. In a confined environment, the phonon dynamics is characterized by revival times for which intense quantum recurrences occur. Mainly due to the ability of the phonons to be reflected by the lattice sides, the initial phonon state is recovered almost periodically. This feature gives rise to the occurrence of a series of dephasing-rephasing mechanisms that restores almost periodically the vibronic coherence. Similarly, under the dipole-dipole interaction, the vibronic coherence is the survival amplitude of

the initial one-vibron state. The vibron dynamics being governed by a discrete energy spectrum, quantum recurrences take place at specific revival times. Nevertheless, since the initial vibron state consists of many eigenstates and because the vibron dispersion is rather large, most of the recurrences give rise to quantum states that slightly resemble the initial state. Therefore, the vibronic coherence behaves as a random variable whose most probable value is zero and intense recurrences correspond to rare events. Consequently, in a statistical sense, the vibronic coherence survives over the vibron correlation time as in an infinite lattice.

In that context a procedure has been established to compare the degree of the vibronic coherence when either the vibron-phonon coupling or the dipole-dipole interaction is turned on. From this procedure, a critical coupling $\chi^*(L)$ has been defined to discriminate between the weak [$\chi < \chi^*(L)$] and the strong coupling limits [$\chi > \chi^*(L)$]. We have shown that $\chi^*(L)$ increases when L decreases, indicating that the vibron-phonon coupling decreases relative to the dipole-dipole interaction when the size of the lattice is reduced. For instance, at biological temperature, $\chi^*(L) \approx 35$ pN for $L=8$ whereas it decays to $\chi^*(L) \approx 25$ pN when $L \rightarrow \infty$.

To conclude, let us mention that in spite of the limitations of the present approach, the two conditions that required to apply our procedure are fulfilled for a lattice of H-bonded peptide units. Indeed, for $L=6$, the lower bound of the adiabaticity is $B_m=0.16$. Fortunately, with the parameters used in our simulation, the adiabaticity is also about $B=0.16$. Nevertheless, small variations in the parameters may provide an adiabaticity smaller than 0.16. Our measure of the coupling strength will remain valid but for a larger lower bound of the lattice size. Therefore, the fundamental question arises whether is it possible to measure the coupling strength when both the lattice size and the adiabaticity become extremely small. This question will be investigated in forthcoming works.

-
- [1] A. S. Davydov and N. I. Kisluka, *Phys. Status Solidi B* **59**, 465 (1973); *Zh. Eksp. Teor. Fiz.* **71**, 1090 (1976) [*Sov. Phys. JETP* **44**, 571 (1976)].
- [2] P. L. Christiansen and A. C. Scott, *Davydov's Soliton Revisited* (Plenum, New York, 1990).
- [3] A. C. Scott, *Phys. Rep.* **217**, 1 (1992).
- [4] A. C. Scott, *Nonlinear Science* (Oxford University Press, New York, 2003).
- [5] D. W. Brown and Z. Ivic, *Phys. Rev. B* **40**, 9876 (1989).
- [6] Z. Ivic, D. Kapor, M. Skrinjar, and Z. Popovic, *Phys. Rev. B* **48**, 3721 (1993).
- [7] Z. Ivic, D. Kostic, Z. Przulj, and D. Kapor, *J. Phys.: Condens. Matter* **9**, 413 (1997).
- [8] W. Forner, *Int. J. Quantum Chem.* **64**, 351 (1997).
- [9] D. Hennig, *Phys. Rev. B* **65**, 174302 (2002).
- [10] V. Pouthier, *Phys. Rev. E* **68**, 021909 (2003).
- [11] C. Falvo and V. Pouthier, *J. Chem. Phys.* **123**, 184709 (2005); **123**, 184710 (2005).
- [12] L. Cruzeiro, *J. Chem. Phys.* **123**, 234909 (2005).
- [13] L. Cruzeiro, *J. Biol. Phys.* **35**, 43 (2009).
- [14] D. V. Tsvilin and V. May, *J. Chem. Phys.* **125**, 224902 (2006).
- [15] D. Cevizovic, S. Zekovic, and Z. Ivic, *Chem. Phys. Lett.* **480**, 75 (2009).
- [16] V. Pouthier and Y. O. Tsybin, *J. Chem. Phys.* **129**, 095106 (2008).
- [17] V. Pouthier, *Phys. Rev. E* **78**, 061909 (2008).
- [18] V. Pouthier, *Phys. Rev. E* **75**, 061910 (2007).
- [19] V. Pouthier, *J. Phys.: Condens. Matter* **21**, 185404 (2009).
- [20] V. Pouthier, *Phys. Rev. B* **80**, 144304 (2009).
- [21] J. Edler, R. Pfister, V. Pouthier, C. Falvo, and P. Hamm, *Phys. Rev. Lett.* **93**, 106405 (2004).
- [22] P. Hamm, *J. Biol. Phys.* **35**, 17 (2009).
- [23] P. Bodis, E. Schwartz, M. Koepf, J. J. L. M. Cornelissen, A. E. Rowan, R. J. M. Nolte, and S. Woutersen, *J. Chem. Phys.* **131**, 124503 (2009).
- [24] H. Fröhlich, *Adv. Phys.* **3**, 325 (1954).

- [25] I. G. Lang and Yu. A. Firsov, *Sov. Phys. JETP* **16**, 1293 (1962).
- [26] D. Yarkony and R. Silbey, *J. Chem. Phys.* **65**, 1042 (1976).
- [27] Z. Ivic, D. Kostic, and D. Kapor, *Phys. Lett. A* **339**, 393 (2005).
- [28] Z. Przulj, D. Cevizovic, S. Zekovic, and Z. Ivic, *Chem. Phys. Lett.* **462**, 213 (2008).
- [29] V. Pouthier, *Phys. Rev. B* **79**, 214304 (2009).
- [30] M. Grover and R. Silbey, *J. Chem. Phys.* **54**, 4843 (1971).
- [31] R. Silbey and R. W. Munn, *J. Chem. Phys.* **72**, 2763 (1980).
- [32] V. Capek and I. Barvik, *J. Phys. C* **20**, 1459 (1987).
- [33] H. Dolderer and M. Wagner, *J. Chem. Phys.* **108**, 261 (1998).
- [34] V. A. Kuprievich, in *Davydov Soliton Revisited*, edited by P. L. Christiansen and A. C. Scott (Plenum, New York, 1990), p. 199.
- [35] B. M. Pierce, in *Davydov Soliton Revisited*, edited by P. L. Christiansen and A. C. Scott (Plenum, New York, 1990), p. 209.
- [36] N. Ostergard, in *Davydov Soliton Revisited*, edited by P. L. Christiansen and A. C. Scott (Plenum, New York, 1990), p. 229.
- [37] V. Pouthier, *J. Chem. Phys.* **132**, 035106 (2010).
- [38] L. Stryer, *Biochemistry*, 4th ed. (W. H. Freeman, New York, 1995).
- [39] J. Wang and J. Feng, *Protein Eng.* **16**, 799 (2003).
- [40] V. May and O. Kuhn, *Charge and Energy Transfer Dynamics in Molecular Systems* (Wiley-VCH Verlag, Berlin, 2000).
- [41] F. Shibata, Y. Takahashi, and N. Hashitsume, *J. Stat. Phys.* **17**, 171 (1977).
- [42] C. Uchiyama and F. Shibata, *Phys. Rev. E* **60**, 2636 (1999).
- [43] H. P. Breuer, B. Kappler, and F. Petruccione, *Phys. Rev. A* **59**, 1633 (1999).
- [44] H. P. Breuer, B. Kappler, and F. Petruccione, *Ann. Phys.* **291**, 36 (2001).
- [45] H. P. Breuer, J. Gemmer, and M. Michel, *Phys. Rev. E* **73**, 016139 (2006).
- [46] H. P. Breuer and F. Petruccione, *The Theory of Open Quantum Systems* (Oxford University Press, New York, 2007).
- [47] S. Welack, M. Schreiber, and U. Kleinekathofer, *J. Chem. Phys.* **124**, 044712 (2006).
- [48] C. Corduneanu, *Almost Periodic Functions* (Chelsea, New York, 1989).
- [49] I. Sh. Averbukh and N. F. Perelman, *Phys. Lett. A* **139**, 449 (1989).
- [50] R. Bluhm, V. A. Kostelecky, and J. A. Porter, *Am. J. Phys.* **64**, 944 (1996).
- [51] M. V. Berry, *J. Phys. A* **29**, 6617 (1996).
- [52] E. J. Amanatidis, D. E. Katsanos, and S. N. Evangelou, *Phys. Rev. B* **69**, 195107 (2004).
- [53] B. Chen, Z. Song, and C. P. Sun, *Phys. Rev. A* **75**, 012113 (2007).